OXFORD

SOT | Society of Toxicology
www.toxsci.oxfordjournals.org

TOXICOLOGICAL SCIENCES, 147(2), 2015, 475–489

doi: 10.1093/toxsci/kfv145
Advance Access Publication Date: July 15, 2015
Research Article

Ethanol Attenuates Histiotrophic Nutrition Pathways and Alters the Intracellular Redox Environment and Thiol Proteome during Rat Organogenesis

Joseph L. Jilek,* Karilyn E. Sant,* Katherine H. Cho,* Matthew S. Reed,† Jan Pohl,† Jason M. Hansen,‡ and Craig Harris*,[1]

*Department of Environmental Health Sciences, University of Michigan, Ann Arbor, Michigan 48109; †Biotechnology Core Facility Branch, Centers for Disease Control, Atlanta, Georgia 30333; and ‡Department of Physiology and Developmental Biology, College of Life Sciences, Brigham Young University, Provo, Utah 84602

[1]To whom correspondence should be addressed at Department of Environmental Health Sciences, University of Michigan, School of Public Health, M6667 SPH II, 1415 Washington Heights, Ann Arbor, MI 48109-2029. Fax: 734 936-7283. E-mail: charris@umich.edu.

ABSTRACT

Ethanol (EtOH) is a reactive oxygen-generating teratogen involved in the etiology of structural and functional developmental defects. Embryonic nutrition, redox environment, and changes in the thiol proteome following EtOH exposures (1.56.0 mg/ml) were studied in rat whole embryo culture. Glutathione (GSH) and cysteine (Cys) concentrations with their respective intracellular redox potentials (E_h) were determined using high-performance liquid chromatography. EtOH reduced GSH and Cys concentrations in embryo (EMB) and visceral yolk sac (VYS) tissues, and also in yolk sac and amniotic fluids. These changes produced greater oxidation as indicated by increasingly positive E_h values. EtOH reduced histiotrophic nutrition pathway activities as measured by the clearance of fluorescin isothiocyanate (FITC)-albumin from culture media. A significant decrease in total FITC clearance was observed at all concentrations, reaching approximately 50% at the highest dose. EtOH-induced changes to the thiol proteome were measured in EMBs and VYSs using isotope-coded affinity tags. Decreased concentrations for specific proteins from cytoskeletal dynamics and endocytosis pathways (α-actinin, α-tubulin, cubilin, and actin-related protein 2); nuclear translocation (Ran and RanBP1); and maintenance of receptor-mediated endocytosis (cubilin) were observed. Kyoto encyclopedia of genes and genomes (KEGG) pathway analysis also identified a decrease in ribosomal proteins in both EMB and VYS. Results show that EtOH interferes with nutrient uptake to reduce availability of amino acids and micronutrients required by the conceptus. Intracellular antioxidants such as GSH and Cys are depleted following EtOH and E_h values increase. Thiol proteome analysis in the EMB and VYS show selectively altered actin/cytoskeleton, endocytosis, ribosome biogenesis and function, nuclear transport, and stress-related responses.

Key words: embryo; visceral yolk sac; organogenesis; ethanol; histiotrophic nutrition; glutathione; cysteine; redox potential; redox environment; thiol proteome

Fetal alcohol syndrome (FAS) and fetal alcohol spectrum disorders (FASD) are well-characterized consequences of *in utero* exposure to ethanol (EtOH), manifest as a variety of clinical conditions. These range from behavioral and cognitive defects (Coriale *et al.* 2013) to craniofacial malformations. However, due to the complex nature of EtOH exposure and timing during development, the precise mechanisms governing the teratogenic activity of EtOH are not well understood. The clinical manifestations of EtOH exposure during organogenesis are believed to include a combination of disrupted cellular and tissue-level processes, including oxidative stress and free radical damage (Dong *et al.* 2008; Miller *et al.* 2013; Miller-Pinsler *et al.* 2015; Smith 1997; Sulik *et al.* 1988), DNA methylation and histone modifications (Kaminen-Ahola *et al.* 2010; Park *et al.* 2003;

Ungerer *et al.* 2013), and dysregulation of microRNA expression (Balaraman *et al.* 2013; Wang *et al.* 2009), among others. Previous studies have identified the damaging potential of EtOH to be related to its ability to promote excess generation of reactive oxygen species (ROS). The specific source of ROS can be traced to products of EtOH biotransformation, release from the mitochondrial respiratory chain or the activation of NADPH oxidases (Dong *et al.* 2010; Hill *et al.* 2014). Due to the spatial and temporal complexities of mammalian embryogenesis, increased concentrations of ROS may originate from various cells and tissues dependent on developmental stage and related metabolic factors. Examples of cell selectivity for EtOH-induced ROS generation include the populations of neural crest cells that actively migrate during early embryogenesis to serve as precursors for nerves, glia, glands, muscle, and several other essential structures. As one of the major targets of EtOH toxicity, perturbation of neural crest cell migration and differentiation strongly correlate with FAS and FASD outcomes. Neural crest cells are known to be deficient in several cellular antioxidant capacities, and it has been suggested that this characteristic contributes greatly to increased ROS accumulation where alterations in the cellular redox environments may be a key step in the general mechanism of the teratogenic effects of EtOH (Davis 1990). The administration of sulforaphane, an inducer of antioxidant responses through Nrf2-mediated pathways, has been shown to provide protection from ROS in neural crest cells (Chen *et al.* 2013). In almost any cellular context, excessive ROS will produce the common consequence of depleting glutathione (GSH) and resulting in the net oxidation of intracellular thiols. Classic definitions of "oxidative stress" would suggest that this overoxidation results only in damaging or deleterious consequences. More contemporary views emphasize the roles of cellular oxidation and reduction as critical signaling elements, which are necessary in normal and abnormal cellular regulation and control (Guttmann 2010; Jones 2006). Characterization of the broader cellular redox environment through the measurement of intracellular redox potentials (E_h) provides a means to compare the magnitude of redox changes in distinct tissues and fluids (Jones 2002) The introduction of a "systems level" thiol proteomics tool allows for the further characterization of what happens to the specific proteins and relevant pathways that are part of the much larger conceptal redox circuitry (Chung *et al.* 2013; Go *et al.* 2014).

A central goal in the current work is to determine the extent to which the redox environments of major conceptal tissues and fluids are altered by EtOH treatment. The numerous reports, including those listed earlier, linking increased generation of ROS and developmental EtOH exposure to mechanisms of adverse functional and anatomical birth defects are instructive but still fall short of describing the complete spectrum of EtOH effects. Perceptions of ROS have changed dramatically over the past decade from an understanding that all ROS are damaging, to the current view that ROS is an essential signaling molecule and second messenger for normal cell regulation and control (Finkel 2011; Guttmann 2010; Hansen and Harris 2013). Most of what ROS does in this capacity is directly linked to its ability to oxidize critical protein cysteine (Cys) sulfhydryl groups in enzyme active sites, receptors, transporters, and transcription factors and thus affect changes in activity and control signaling. The scope of changes to these signaling nodes is extensive and complex and can be differentially impacted by the specific chemical or insult causing the change in ROS status. These are occurring in conjunction with a general reprogramming of genetic networks resulting from EtOH exposure (Green *et al.* 2007) One, often underappreciated, factor that affects ROS-mediated outcomes in cases such as EtOH exposure, is the nutritional state of the exposed organism, having an impact on the type and quantity of proteins being synthesized during embryogenesis and their functional states once formed (Dreosti 1993).

During the sensitive period of organogenesis, both rodent and human conceptuses are undergoing rapid growth and differentiation in a relatively hypoxic environment prior to the establishment of a fully functional placenta (Harris *et al.* 2013). In the rodent and also likely in the human, nutrients are supplied through the visceral yolk sac (VYS) (Burton *et al.* 2001), which actively takes up maternal proteins by receptor-mediated endocytosis (RME) and degrades them via lysosomal proteolysis (Harris *et al.* 2013). These 2 processes constitute the histiotrophic nutrition pathways (HNP) which provide micronutrients to the embryo (EMB) for all of its biosynthesis and metabolism needs during organogenesis (Beckman *et al.* 1998; Christensen and Birn 2002). Disruption of HNP by environmental or chemical agents has been shown to contribute to significant growth retardation and dysmorphogenesis (Ambroso and Harris 1993; Brent *et al.* 1990). Chemical toxicants are known to affect the supply of necessary amino acids required for protein and nucleic acid biosynthesis in the developing EMB. Recent work has also confirmed that reductions in amino acid supply also significantly increases ROS generation (Ambroso *et al.* 1997; Arriazu *et al.* 2010). Two major consequences of reduced amino acid availability are reduced protein biosynthesis and reduced *de novo* GSH biosynthesis. These outcomes are linked by changes in the quantity of conceptal proteins and the functional quality of remaining proteins regarding their cysteine redox status. Systems level assessment of qualitative changes to the thiol proteome (Fu *et al.* 2008) will allow us to identify additional specific pathways and proteins most affected by EtOH exposure.

To better understand the mechanistic consequences of embryonic EtOH exposure, we have, in this report, attempted to integrate information gathered from multiple experimental platforms. We provide the backdrop of a concentration dependent morphology assessment in whole embryo culture (WEC) and a detailed evaluation of GSH and Cys redox profiles. Under similar WEC conditions, we also show EtOH-induced decreases in the histiotrophic uptake of proteins and correlate these with systems level changes to the thiol proteome in EMB and VYS. Combined, these data help to integrate toxin-induced changes to proteins and their associated functional pathways through oxidative posttranslational modifications for an improved understanding of EtOH embryotoxicity that integrates ROS, nutrition, and proteomic changes.

MATERIALS AND METHODS

Chemicals and reagents. GSH, glutathione disulphide (GSSG), cysteine, cysteine (CySS), gamma-glutamyl-glutamate, iodoacetic acid, iodoacetamide, bicinchoninic acid (BCA), fluorescein isothiocyanate albumin conjugate (bovine; fluorescin isothiocyanate [FITC]-albumin), Triton X-100, tri-choloroacetic acid, sodium hydroxide, and sodium dodecylsulfate were purchased from Sigma-Aldrich (St. Louis, Missouri). Dansyl chloride was purchased from Fluka Chemie/Sigma-Aldrich. EtOH (200 proof) was purchased from Decon Labs, Inc (King of Prussia, Pennsylvania). Chloroform and sodium phosphate were purchased from Fisher Scientific (Pittsburgh, Pennsylvania). Hanks balanced salt solution (HBSS) and penicillin/streptomycin (10 000 units/ml penicillin + 10 000 μg/ml streptomycin in 0.85% saline) were purchased from GIBCO/Life Technologies (Grand Island, New York). Cleavable isotope coded affinity tag

(ICAT) reagent kits were purchased from AB Sciex/Applied Biosystems (Framingham, Massachusetts).

Animals. All experiments were conducted in rat WEC (rWEC) using gestational day (GD) 10–11 conceptuses obtained from primagravida time-mated and specific pathogen free Sprague Dawley rats purchased from Charles River Laboratories (Portage, Michigan). A sperm-positive vaginal smear on the morning following mating was used to confirm pregnancy and was used to designate GD 0. Pregnant dams were shipped 4–5 days prior to use, housed in solid bottom polycarbonate cages with corn cob bedding, maintained on a 12-h light/dark room cycle, and were allowed access to standard commercial rodent diet and water *ad libitum*.

Culture conditions, exposure, and sampling. Anesthesia, exsanguination, and uteri removal were conducted as previously described, in accordance with approved institutional animal care and use protocols (Harris *et al.* 2013). Immediately following euthanasia of GD 10 pregnant dams, uteri were removed, placed in HBSS (pH 7.4), and each implantation site was removed using forceps and irridectomy scissors. Decidual masses were opened using fine watchmakers forceps under HBSS and completely intact conceptuses were removed. Reichert's membranes were torn away using fine watchmakers forceps and viable conceptuses, with intact VYS and ectoplacental cones, were transferred into 10 ml of warmed culture medium (not exceeding 1 conceptus per milliliter of culture medium). Prior to addition of conceptuses, culture bottles were saturated with 20% O_2, 5% CO_2, and 75% N_2 and medium was warmed to 37°C. Culture media consisted of heat-inactivated rat serum (50%), HBSS (pH 7.4, 50%), and 43 µl of penicillin/streptomycin. Culture media was resaturated with 95% O_2, 5% CO_2 after 20 h of culture (GD 11) to ensure optimal growth and development. Prior to morphology assessment and other functional characterizations in GD 11, conceptal viability was confirmed by the presence of an active heartbeat and vitelline blood circulation.

Three different EtOH treatment paradigms were used in these studies. For all concentration response, morphology assessment, and redox profiling protocols EtOH at concentrations of 1.5, 3.0, or 6.0 mg/ml was added directly to the culture media containing conceptuses at the onset of the culture period (GD 10) and remained in the media for the entire 26-h period prior to harvesting and evaluation. HNP evaluations and exposures for assessment of the thiol proteome were initiated on GD 11 after approximately 20 h in culture as described later.

Morphology assessment. Assessment of overall changes to conceptal growth and EMB morphology were made following a 26-h exposure of conceptuses to EtOH (1.5, 3.0, and 6.0 mg/ml) in WEC using a scoring protocol outlined in detail previously (Harris 2012). Exposure ranges were chosen based on previous WEC experiments where it was determined that anatomical lesions were first detected at 6 mg/ml and viability was lost at EtOH concentrations in excess of 12 mg/ml. Concentrations of 1.5 mg/ml are believed to be close to concentrations found in human fluids at the legal limits of intoxication (0.1–0.8 mg/ml) for many countries (ICAP Blue Book, International Center for Alcohol Policies). [http://www.icap.org/policytools/icapbluebook/ bluebookmodules/16bloodalcoholconcentrationlimits/tabid/176/default.aspx]. Determinations of EMB and VYS protein contents using the BCA assay procedure (Kirlin *et al.* 1999) were also made as a confirmation of EtOH effects on overall conceptal growth.

Analysis of histiotrophic nutrition. Whole conceptuses were explanted and cultured as indicated earlier for 24 h. Following the culture period, histiotrophic clearance of nutrients was measured as demonstrated previously (Ambroso and Harris 2012). Briefly, FITC-albumin was added to each culture bottle on GD 11 at a concentration of 100 µg/ml culture media. Culture bottles were incubated for 3 h, and whole conceptuses were removed, rinsed in HBSS, and placed in a drop of 250 µl cold 50 mM sodium phosphate buffer (pH 6.0) on a plastic culture dish. Entire VYS and EMB samples were collected following agitation, rinsed in HBSS, and placed in 250 µl of 0.1% Triton X-100. The remaining fluid was collected (consisting of the extraembryonic fluids; EEF). Samples were sonicated, measured for protein concentration by BCA assay (Kirlin *et al.* 1999) precipitated by 750 µl of 6% trichloroacetic acid (TCA), and stored for 1 h prior to centrifugation. TCA-soluble supernatants were separated from the pellet and 1 ml of 500nM Tris buffer and 150 µl of 1N NaOH were added to bring the pH to approximately 8.8. TCA-insoluble pellets were solubilized with 150 µl of 1N NaOH, vortexed, and allowed to incubate at room temperature for 1 h. Following, 1 ml of 500 mM Tris buffer, 150 µl of 1N NaOH, and 750 µl of 6% TCA were added to each sample. Aliquots of the culture media were collected, total protein was determined by BCA assay, and diluted in 250 µl of 0.1% Triton X-100, 750 µl of 6% TCA containing 1% SDS, and 150 µl of 1N NaOH. TCA-soluble and TCA-insoluble components were collected as mentioned earlier. Fluorescence for TCA-soluble, TCA-insoluble, and all media and "blank" samples was measured in a black polypropylene 96-well plate and read using an excitation wavelength of 495nm and an emission at 520nm, using a standard curve composed of a 1:10 000 dilution of FITC-albumin balanced for pH by 500 mM Tris buffer and 6% TCA (Ambroso *et al.* 1997; Ambroso and Harris 2012).

Analysis of soluble thiol concentrations and redox potential calculation. Tissue and fluid compartment samples were collected on GD 11 from cultured rat embryos as indicated earlier, following the 26-h incubation period. One or two intact conceptuses were collected in a 150 µl drop of cold HBSS and the VYS were torn open without rupturing the amnion, and gently agitated to disperse yolk sac fluid (YSF) into the drop. The drop was collected and added to an equal volume of 2 × high-performance liquid chromatography (HPLC) preservation buffer containing 10% perchloric acid, 0.4 M boric acid, and 20 µM γ-glutamylglutamate (γ-EE). One hundred and fifty microliters of cold HBSS was added to reconstitute the drop and the VYS were lifted using fine watchmakers forceps and placed in 300 µl of 1× HPLC preservation buffer containing 5% perchloric acid, 0.2 m boric acid, and 10 µM (γ-EE). The amnion was then removed to disperse the amniotic fluid (AF) into the drop and the EMB was placed in 300 µl 1× HPLC preservation buffer. The remaining drop containing the AF was collected and combined with an equal volume of 2× HPLC preservation buffer. All samples were immediately snap frozen following collection and saved at −74°C prior to HPLC analysis.

Sample derivitization for HPLC was conducted as described previously by Jones (2002) and as modified by Harris and Hansen (2012). Samples were then thawed and prepared by ultrasonic cell disruption followed by centrifugation and pelleting of precipitated protein (14 000 × g for 10 min). The supernatant was then removed and the pellet was solubilized in 1 ml 250 mM sodium hydroxide for total protein determination by (BCA) assay, standardized to a series of known bovine serum albumin solution (Kirlin *et al.* 1999). The supernatant was

reacted with 60 ml iodoacetic acid (14.8 mg/ml) to block all accessible thiol groups and the pH was adjusted to 9.0 using saturated (1 M) potassium tetraborate. Samples were left to stand for 20 min. Amino groups were labeled by the addition of 300 ml dansyl chloride (20 mg/ml in acetone) and samples were allowed to react at room temperature overnight in the dark. Derivitization was completed with the addition of 500 ml chloroform followed by mixing, centrifugation, and removal of the top sample layer that contains the thiols of interest.

GSH, GSSG, cysteine, and cystine were resolved and quantified using reverse-phase HPLC analysis on a Waters 2695 Alliance Separations Module fitted with a Supelcosil LC-NH_2 column (Sigma-Aldrigh). Mobile phases consisted of (1) 80% methanol and 20% ddiH_2O and (2) 62.5% methanol, 12.5% glacial acetic acid and 214 mg/ml sodium acetate trihydrate in ddiH_2O in a gradient at a flow rate of 1 ml/min. Detection of peaks was made using a Waters 2474 fluorescence detector (excitation 335nm and emission at 518nm).

Calculation of redox potentials from HPLC data using the Nernst equation required the calculation of concentrations for each of the thiols of interest separated by this method, previously explained by Harris *et al.* (2013). Briefly, volumes of tissues and fluid compartments for the calculation of concentrations were estimated using 2 methods. Tissue concentrations for thiols in the VYS and EMB were estimated from total tissues protein using the BCA assay, using bovine serum albumin as an authentic standard. Fluid volumes in the YSF and AF compartments were estimated from average digital measurements of a GD 11 conceptus determined using NIH Image software. Approximate volumes using the various spheres (VYS, amnion, and EMB) were calculated using the equation $4\pi r^3$ and sequentially subtracting compartments to find the difference. Final data is, thus, expressed as absolute thiol concentrations and redox potentials (E_h) calculated from the Nernst equation.

Thiol proteome analysis using cleavable ICAT reagents. Whole GD 10 conceptuses were explanted and cultured to GD 11 as described earlier. All conceptuses were regassed according to standard protocols (20 h of culture) after which 6.0 mg/ml EtOH was added directly to designated bottles for an exposure period of 6 h. EMB and VYS samples were obtained at the conclusion and processed for ICAT analysis as previously described (Harris *et al.* 2013) and according to the manufacturer's instructions (AB Sciex/Applied Biosystems). Cleavable isotope-coded affinity tags reagents are designed to covalently bond to a specific functional group on proteins. The reagents used here employ the maleimide group of the tag to specifically bind all reduced cysteine residues on proteins following global disulfide reduction with tris (2-carboxyethyl) phosphine. The samples are then digested with trypsin and the resulting peptides are enriched using the biotin moiety via separation on an avidin column. After enrichment, the biotin tag is removed, by the acid linker, and the remaining peptides remain bound only to maleimide and the stable carbon isotopes. The control samples are labeled with the (**L**)ight ^{12}C-isotope and the treated samples are labeled with the (**H**)eavy ^{13}C isotope and the 2 peptide samples are mixed prior to analysis. Mass spectroscopy analysis will resolve each tagged peptide in tandem and allow for the direct calculation of H/L ratios and, following peptide sequence analysis, the relative concentrations of identified proteins. A 100 μg sample of both untreated control and 6.0 mg/ml EtOH-treated EMB and VYS samples were labeled with the maleimide ICAT reagents. Untreated control samples were labeled with the ^{12}C (light) isotope and 6.0 mg/ml EtOH-treated samples were labeled with the ^{13}C (heavy) isotope, to directly compare treatment-related changes in relative protein abundance. Labeled peptide samples were prepared for mass spectrometry and analyzed as previously described (Harris *et al.* 2013) per instructions provided by the manufacturer (Applied Biosystems). Identification of proteins by tryptic peptide fragment analysis and evaluation of H/L ratios were used to compare protein quantities as also described previously (Harris *et al.* 2013). The principle output from an ICAT analysis following trypsin digestion and resolution by mass spectroscopy was the H/L ratio. Only ratios that varied from unity by more than 15% were considered to be significantly different. Proteins meeting these criteria were interrogated using the Kyoto encyclopedia of genes and genomes (KEGG) pathway database (http://www.genome.jp/kegg) to predict functional pathway associations and links among proteins. Only proteins for which pathway data is available in KEGG were used in this study. Further details of the analysis procedure can be found in (Harris *et al.* 2013)

Statistical analysis. Representative values in this report are expressed as the mean ± standard error of the mean (SE). A confidence level of 95% ($\alpha = .05$) was used as the threshold for statistical significance. Statistical outliers were excluded from analysis after meeting the criteria of being 1.5 times the interquartile range outside of the first and third quartile measures. All measures were compared using Student's *t* tests and ANOVA using Tukey's *post hoc* test to determine statistical significance (IBM SPSS).

RESULTS

Morphology Assessment

Results from the morphology assessment showed that EtOH exposure in WEC at concentrations from 1.5 to 3.0 mg/ml had no significant pairwise effects on overall growth and development in terms of the scoring of anatomical characteristics or total protein content in EMB and VYS (Fig. 1). At EtOH concentrations of 6.0 mg/ml, morphology scores were significantly reduced by 15% and EMB protein was decreased by more than 45%. No significant changes were seen in VYS protein concentrations, indicating a selective effect on the EMB proper. Anatomical changes at the higher concentrations were limited to incomplete axial rotation and some hyperplasia of the prosencephalon.

Histiotrophic Nutrition Pathways

Following the 20-h culture period, clearance of fluorescence from the culture media into the conceptus was measured through addition of FITC-albumin to the culture media. Following the 3-h incubation period with EtOH and FITC-albumin, clearance was measured by fluorometric analysis of the culture media, VYS, EEF, and EMB. Total clearance into the entire conceptus was found to decrease in a concentration-dependent manner, expressed as a nearly 50% decrease from control values at the highest concentration (6.0 mg/ml) (Fig. 2). Due to the short incubation period, the majority of FITC was measured in the VYS and EEF (Ambroso *et al.* 1997).

Total clearance into each tissue or fluid compartment was measured as a sum of acid-soluble and acid-insoluble FITC, prior to analysis for fluorescence. The fraction of clearance of

	Morphology Score	Protein (µg) VYS	EMB
CONTROL	93.8	86.3 ± 4.7	155.6 ± 9.8
ETHANOL 1.5 MG/ML	92.1	92.7 ± 5.8	134.5 ± 7.3
ETHANOL 3.0 MG/ML	87.7	89.8 ± 6.3	134.3 ± 12.2
ETHANOL 6.0 MG/ML	79.5*	77.3 ± 7.0	86.2* ± 12.1

FIG. 1. Morphology assessment and protein determination as a measure of overall growth. Ethanol (EtOH) was added directly to the culture medium containing intact gestational day (GD) 10 conceptuses at concentrations of 1.5, 3.0, and 6.0 mg/ml and cultured for 26 h under standard whole embryo culture (WEC) conditions. On GD 11 conceptuses were scored for growth and dysmorphogenesis using our complete morphology assessment protocol (Harris 2012). Total embryo (EMB) and visceral yolk sac (VYS) protein were measured using the bicinchoninic acid assay as described in Materials and Methods. An * denotes values significantly different from control ($p < .05$) with $n = 10$ conceptuses for each group.

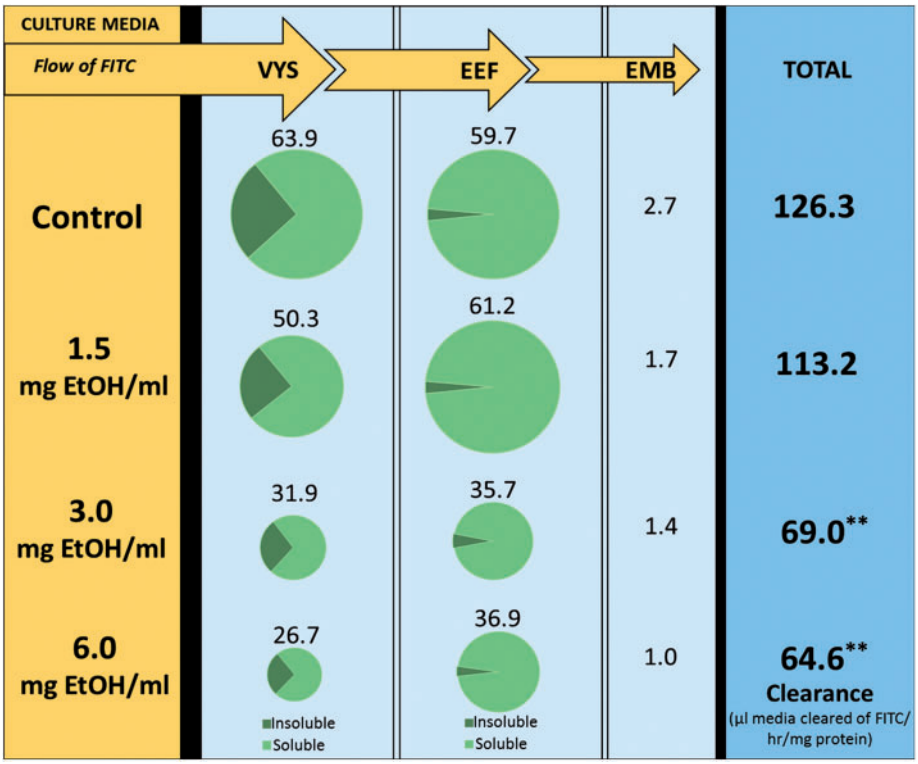

FIG. 2. Histiotrophic nutrition assay, indicating clearance of fluorescin isothiocyanate (FITC)-albumin to VYS, extraembryonic fluid, and EMB from culture media. Uptake of FITC-albumin from culture media was assayed over a 3-h exposure period on GD 11. Clearance is defined as: µl of media cleared of FITC/h/mg protein as described in Materials and Methods. All measurements were standardized to total protein. trichloroacetic acid (TCA)-soluble and TCA-insoluble fractions were measured in each compartment to indicate the amount of degraded or whole protein, respectively. The relative proportions of total cleared FITC are represented by pie charts along with the total clearance value for both soluble and insoluble fractions. ** Indicates significant decrease in FITC compared with control at $p < .01$.

FITC into the VYS was approximately 25% acid-insoluble and 75% acid-soluble at all concentrations, suggesting that proteolysis (and subsequent cargo release) of the endocytotic vesicles into this tissue occurs at the same rate and efficiency independent of EtOH concentration. Furthermore, this is also observed in the EEF, where the acid-insoluble fraction of FITC constitutes approximately 3%–6% of the total clearance into this compartment.

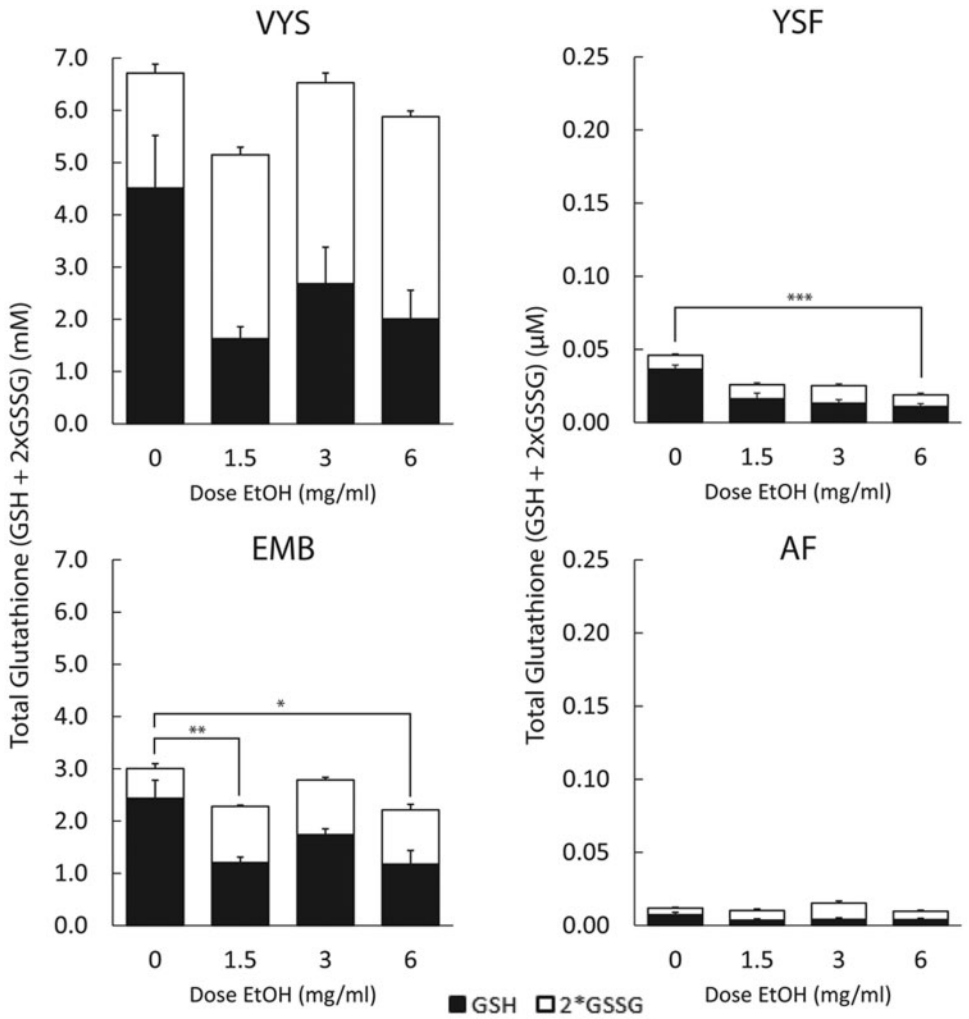

FIG. 3. Total GSH measured by high-performance liquid chromatography (HPLC) analysis (Materials and Methods) and calculated by the sum of reduced GSH (filled bars, [GSH]) and oxidized glutathione (open bars, 2*[GSSG]). SE bars represent respective GSH and glutathione disulfide (GSSG) concentrations; total glutathione ([GSH]+[GSSG]) values were compared between each group by ANOVA and Tukey's *post hoc* tests. * Indicates significant difference at $p < .05$ when compared with control; ** indicates $p < .01$ when compared with control; *** indicates $p < .001$ when compared with control.

Total GSH and Cys

Absolute GSH and Cys concentrations were measured by HPLC at concentrations of 0, 1.5, 3.0, and 6.0 mg/ml EtOH, and total GSH and Cys were calculated according to the formula GSH + 2GSSG or Cys + 2CySS, respectively, to account for stoichiometry of dithiols (Figs. 3 and 4). In the VYS, total Cys remained unaltered with respect to control, except at the highest concentration, in which a significant decrease in total Cys from 0.59 ± 0.06 mM to 0.43 ± 0.03 mM was observed. Total GSH levels did not change significantly in the VYS.

Total GSH in the YSF showed a slight decreasing trend over all concentrations, whereas total Cys displayed an increasing trend toward significance at the intermediate concentration when compared with control (from 0.58 to 0.83 µM), but then significantly decreased at the highest concentration (0.40 ± 0.04 mM). In the AF, total GSH and Cys did not change significantly, although an overall decreasing trend of total Cys was observed at the highest concentration, from 0.09 ± 0.02 mM to 0.07 ± 0.01 mM. Generally speaking, these data suggest that when the complete redox pair was observed simultaneously, total Cys was impacted to a greater extent than total GSH.

Reduced and Oxidized GSH

Within the VYS, GSH decreased nonuniformly from control levels at all EtOH concentrations (Fig. 5). GSSG concentrations increased very significantly from control, reaching a uniform maximum of approximately 1.9 mM. This pattern is consistent with the adjacent fluid compartment of the YSF where GSSG increases then remains relatively constant at all concentrations compared with control levels. This may be a consequence of GSH oxidation in the VYS, and the subsequent induction of GSH shuttling from the YSF into the VYS in an effort to maintain intracellular GSH levels.

Embryonic GSH levels also decrease relative to controls by approximately 50% in both 1.5 and 6.0 mg/ml EtOH concentration groups, and by a factor of approximately 0.25 in the 3.0 mg/ml EtOH concentration group (Fig. 5). GSSG increased approximately 2-fold at all concentration groups when compared with control levels, with very little variation. Reduced GSH levels become significantly decreased at higher contrentations of EtOH, however, these levels are in the micromolar range and contribute less to supporting embryonic GSH homeostasis. Furthermore, when compared with total GSH, GSSG accounts for more than half of the total at all concentrations of EtOH,

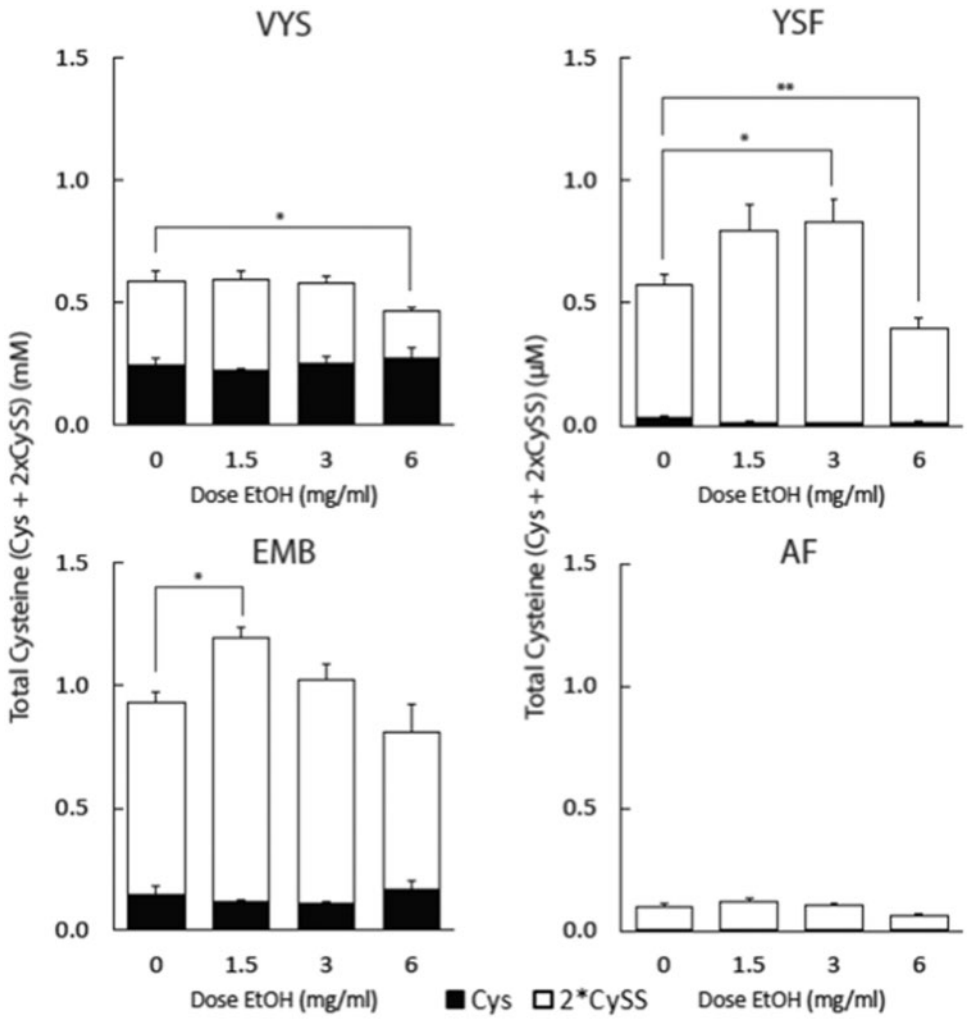

FIG. 4. Total cysteine measured by HPLC analysis (Materials and Methods) and calculated by the sum of reduced cysteine (filled bars, [Cys]) and oxidized cystine (open bars, 2*[CySS]). SE bars represent respective Cys and CySS concentrations; total cysteine ([Cys]+[CySS]) values were compared between each group by ANOVA and Tukey's *post hoc* tests. * Indicates significant difference at $p < .05$ when compared with control; ** indicates $p < .01$ when compared with control; *** indicates $p < .001$ when compared with control.

while the opposite is true in the control samples; this observation is reflected in the VYS at very similar ratios.

Reduced and Oxidized Cys

Reduced and oxidized Cys in the VYS remains fairly constant across all concentrations of EtOH, although CySS is significantly decreased at 6.0 mg/ml EtOH, from a control level of 0.29 ± 0.03 mM to 0.46 ± 0.02 mM (Fig. 6). This is accompanied by a decrease in total Cys in the same group, possibly due to an inhibition of amino acid supply as previously indicated. Additionally, as the primary soluble thiol within fluid compartments, CySS levels in the YSF were shown to have increased significantly at 1.5 and 3.0 mg/ml EtOH concentrations but decreased significantly from control levels at the 6.0 mg/ml EtOH dose.

Redox Potentials

Absolute reduced and oxidized GSH and Cys concentrations were used in the Nernst equation to calculate the respective redox potentials (E_h) for tissues and fluids using data from the GSH/GSSG and Cys/CySS redox couples (Fig. 7). Initial E_h values in VYS and EMB were −207 and −216 mV, respectively, showing the EMB to be the more reducing environment. The GSSG/GSH redox potential (E_h) was found to become more positive (more oxidizing) at all EtOH concentrations and this alteration was fairly consistent between each fluid compartment and tissue. Additionally, these effects on E_h were most significant at the lowest concentration level (1.5 mg/ml EtOH) and remained at similar levels with increasing concentration. A similar trend was found when examining the CySS/Cys E_h, however, this effect was largely confined to YSF and AF and the increase was not as robust. CySS/Cys redox potentials in the VYS and EMB at the 6.0 mg/ml EtOH concentration level were found to have either increased significantly or remained the same, respectively, from control values. However, this discrepancy is also reflected in decreased total Cys, as CySS levels in both cases were decreased and Cys levels did not change as much from control levels.

Thiol Proteome

Proteins with accessible thiol groups were labeled with isotope-coded affinity tags to quantify the relative change in abundance, with respect to control groups, at the 6.0 mg/ml EtOH concentration group. Paired resolution of identical heavy and

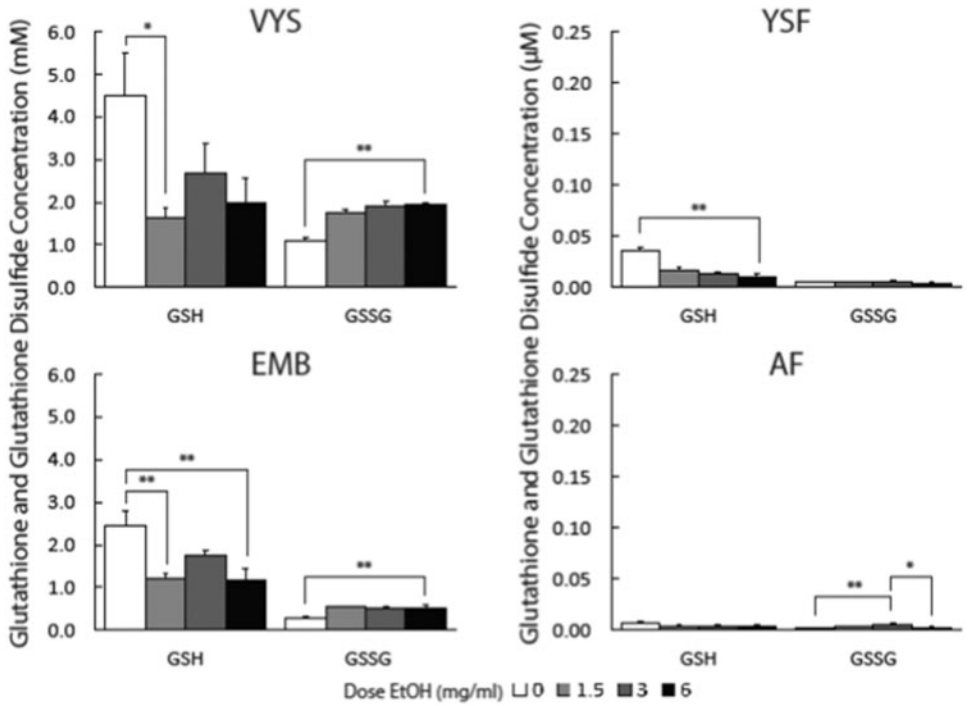

FIG. 5. Changes to reduced and oxidized glutathione (GSH and GSSG, respectively) were compared across untreated and EtOH-exposed conceptuses at various concentrations. All rat conceptuses were allowed to grow for 24 h before processing and subsequent derivatization (Materials and Methods). GSSG concentrations in both EMB and VYS tissues are significantly increased at all concentrations of EtOH. * Indicates significant difference at $p < .05$; ** indicates $p < .01$.

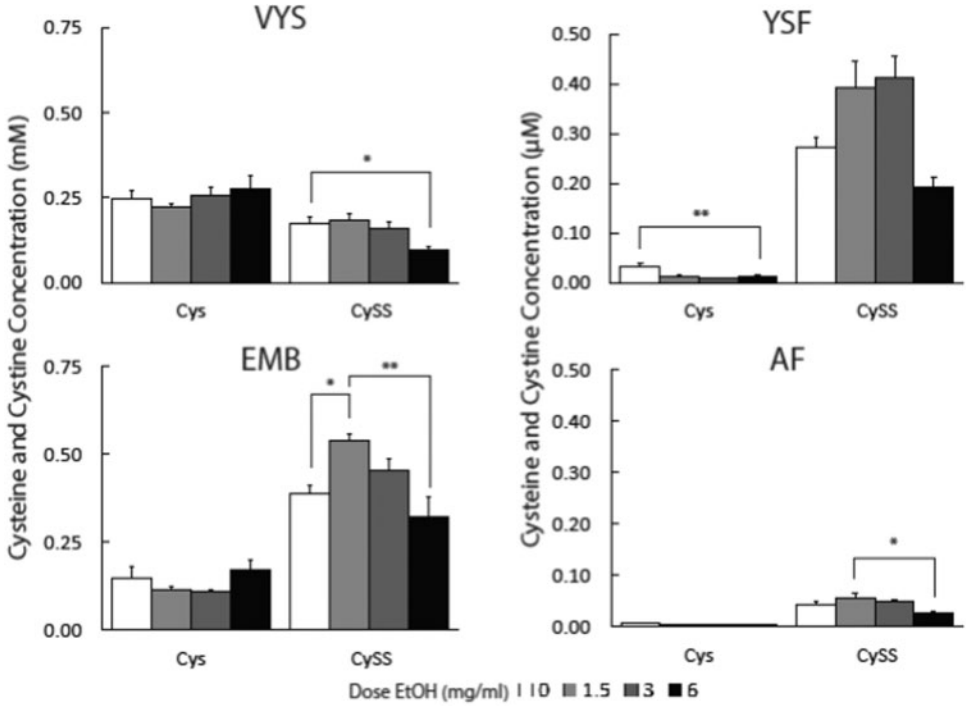

FIG. 6. Changes to reduced and oxidized cysteine (Cys and CySS, respectively) were compared across untreated and EtOH-exposed conceptuses at various concentrations. All rat conceptuses were allowed to grow for 24 h before processing and subsequent derivatization (Materials and Methods). * Indicates significant difference at $p < .05$; ** indicates $p < .01$.

light isotope tagged peptides by mass spectrometry and the subsequent identification of their proteins of origin by tryptic peptide analysis made the ratiometric analysis possible. A shift in the H/L ratio was indicative of an absolute change in protein abundance within the thiol proteome in both EMB and VYS tissues. Proteins with an H/L shift > 15% were included in the analysis, which shows an overall trend toward decreased concentration-related abundance in the VYS and increased

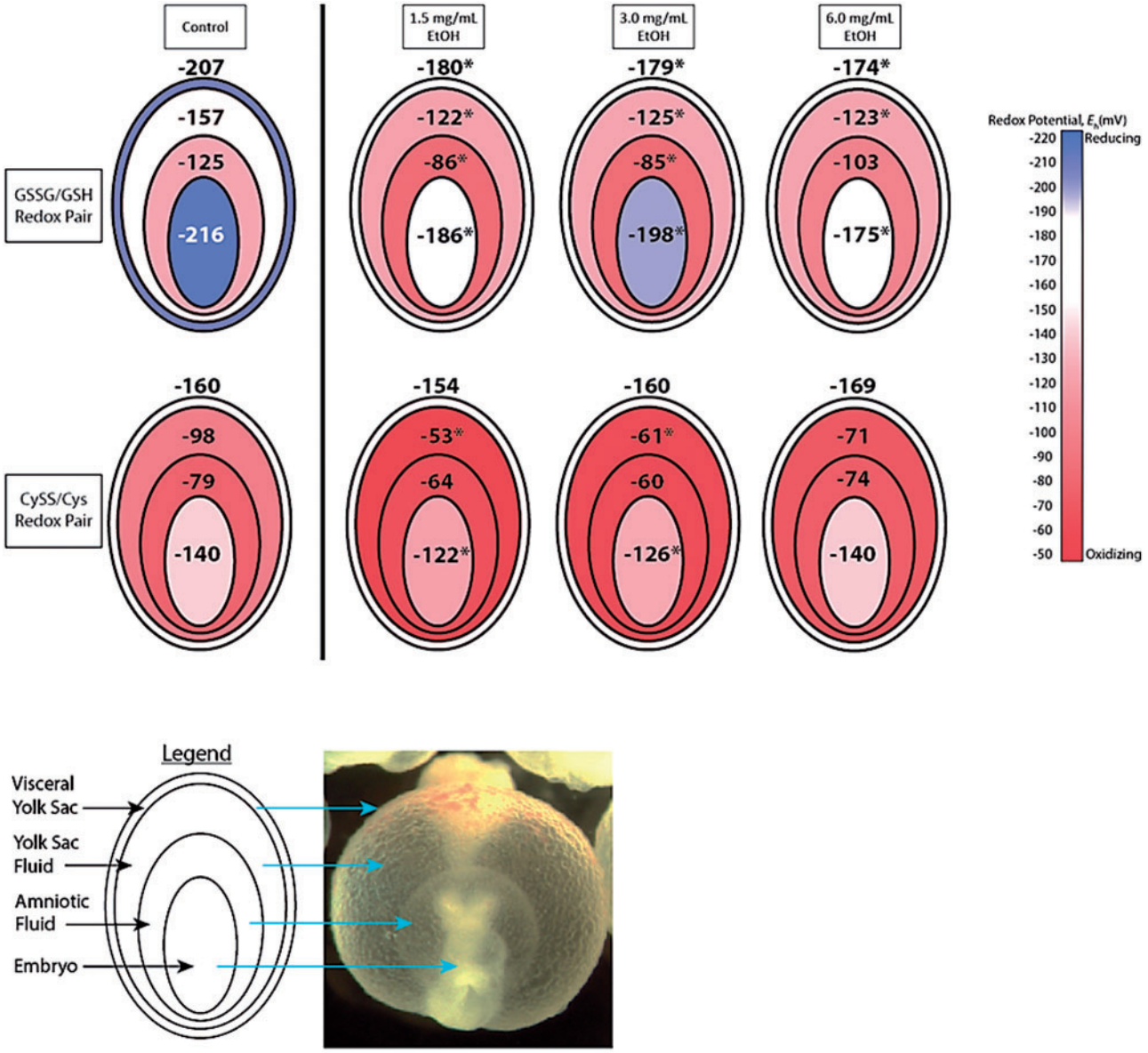

FIG. 7. Redox potentials (E_h) for the GSH and Cys redox couples in major tissue (VYS, EMB) and fluid (yolk sac fluid, amniotic fluid) compartments of the intact conceptus are shown following 26-h exposure to EtOH at concentrations of 1.5, 3.0, and 6.0 mg/ml in WEC. GSH, GSSG, Cys, and CySS were measured directly by HPLC and E_h calculated using the Nernst equations described in Materials and Methods. Diagrams show the spatial and anatomical relationships between tissue and fluid compartments along with their respective E_h values expressed in mV units. Color coding provides improved visualization of redox changes and patterns in tissues and fluids where progression to blue represents more reducing environments and progression to red showing more oxidizing conditions. An * denotes values that are significantly different at $p < .05$ when compared with their appropriate controls. Full color version available online.

concentration-related abundance in the EMB. Specifically, in the VYS, proteins involved in actin cytoskeleton dynamics and RME were found to have reduced abundance. In both EMB and VYS, proteins associated with nuclear transport (Ran pathway) were reduced and α-fetoprotein was increased (Fig. 8).

ICAT data were also analyzed using a pathway analysis, including proteins that changed in relative abundance by at least 15% from control (based upon the H/L ratio). Based upon the total data, a majority of changes in relative abundance occurred in the VYS (72 changes), fewer were observed in the EMB (24 changes), and 16. Of the specific pathway changes identified, 16 were common between both VYS and EMB (Fig. 9). Notably, the largest altered pathways were ribosomal proteins in the VYS, accounting for 14 changed pathways in all (Fig. 8).

DISCUSSION

EtOH is a well-known developmental toxicant and teratogen that has been shown to affect a broad spectrum of biochemical and molecular pathways leading to both functional and anatomical defects. Animal models of EtOH teratogenicity, including the rat WEC model used in these studies have revealed a number of significant endpoints that are altered directly or indirectly following exposure. Drawing conclusions regarding the mechanistic relatedness of multiple observations across different species and models is very difficult and has led to the design

Visceral Yolk Sac

Protein	H/L	Description
Decreased Relative Abundance		
α-actinin-4	0.48	Focal adhesion assembly, formation of tight junctions, regulation of actin cytoskeleton
Ran GTPase	0.71	Nuclear transport factor (tRNA, rRNA export)
Actin-related protein 2	0.76	Nucleation of new actin filaments
Cubilin	0.79	Vitamin digestion and absorption
Tubulin α-4A	0.83	Phagosome, formation of gap junctions
Profilin	0.84	Regulation of actin cytoskeleton (actin polymerization)
Thioredoxin	0.85	
Increased Relative Abundance		
α-fetoprotein	1.31	Binds copper, nickel, fatty acids, and low levels of estrogen

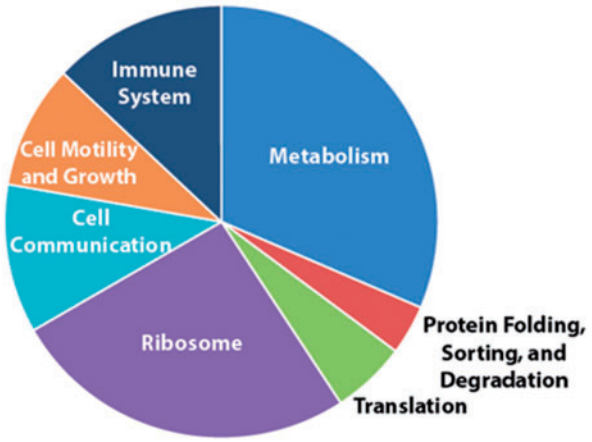

Embryo

Protein	H/L	Description
Decreased Relative Abundance		
RanBP1	0.79	Ran cycle regulation
Increased Relative Abundance		
Tubilin α-4A	1.15	Phagosome, formation of gap junctions
Stress-induced-phosphoprotein 1	1.23	Linkage of Hsp70 and Hsp90
Protein disulfide isomerase	1.35	Formation/dissociation of thiol groups and disulfide bonds
α-fetoprotein	1.62	

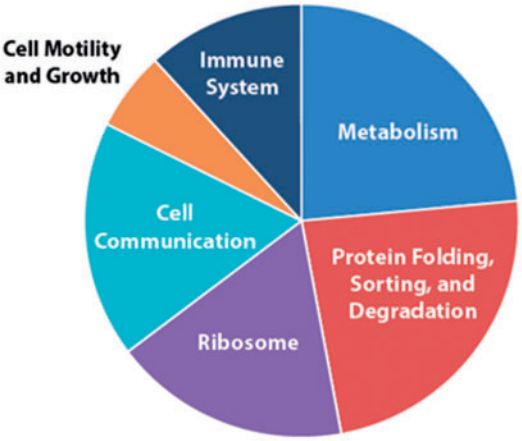

FIG. 8. Relevant changes in protein abundance within the thiol proteome. Proteins with accessible thiol groups were differentially labeled with cleavable isotope coded affinity tag reagents and resolved by mass spectroscopy. The 6.0 mg/ml EtOH-treated group was tagged with heavy isotopes and the untreated control group was tagged with light isotopes. Heavy-to-light (H/L) ratios were calculated from mass spectroscopy data, where H/L values < 1 indicate treatment-related decreases in protein abundance, and H/L values > 1 indicate treatment-related increases in protein abundance. This chart is a selection of relevant proteins, given the criteria that relative protein abundance differs by at least 15%. Pathway analysis in EMB and VYS tissues was compiled using the Kyoto encyclopedia of genes and genomes (KEGG) database. Proteins were included in this analysis given that relative abundance differed by at least 15%.

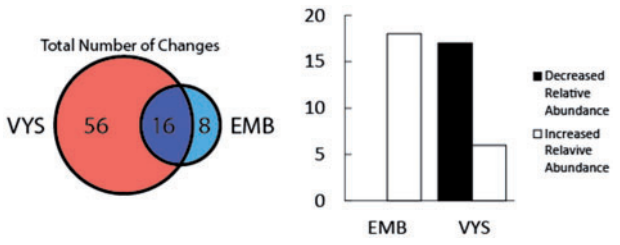

FIG. 9. Summary of pathway analysis, indicating relevant changes to VYS, EMB, and overlapping pathways. Proteins were included given that relative abundance differed by at least 15% and the KEGG database was used to identify pathways. B, Relevant proteins used in the pathway analysis were compared using h/l ratios to indicate decreases or increases in relative abundance. The majority of alterations were identified in the VYS and accounted for all of the negative changes to relative abundance at the 15% change in h/l standard.

of studies that integrate different methodologies and platforms to help identify relevant points of mechanistic intersection. These include high throughput "systems biology" approaches to improve our understanding of complex and overlapping interactions. In this report, we have combined a standard dose-response morphology assessment with GSH and Cys redox profiling, HNP assessment, and systems level thiol proteomics analysis to better elucidate the effects of EtOH exposure on organogenesis-stage rat conceptuses at a biochemical level. Integration and interpretation of results show several areas of congruence where alterations to a subset of pathways and processes are closely related to nutrient uptake deficits, ROS generation, and the regulated control of cellular adaptation/survival pathways collectively associated with autophagy.

Clear evidence of EtOH-induced dysmorphogenesis in rat conceptuses grown in WEC is not apparent below concentrations of 6.0 mg/ml. Approximately 70% of EMBs exposed to this concentration of EtOH appear to be unaffected by treatment based on morphology but can be shown to exhibit significant functional alterations even at the lowest concentrations tested. This is in agreement with other studies that show EtOH developmental toxicity to present with greater functional deficits than with morphological changes (Mukherjee *et al.* 2006). The functional changes assessed here, include a broader quantitative assessment of EtOH alterations to the nutritional state; conceptal RME activity and consequences of increased ROS generation; detailed assessment of the thiol redox status in EMB and VYS. The separate evaluation of VYS and EMB tissue compartments is important and often overlooked because nutrient

uptake, metabolism, and redox control are intimately regulated between these 2 compartments of the developing conceptus.

The major source of amino acids required for fuel and the supply of anabolic precursors for biosynthesis in the conceptus during organogenesis comes through HNP via the inverted VYS. Whole proteins and their associated cargoes are taken up by RME at the VYS brush border, incorporated into primary endocytotic vesicles, and fused with lysosomes where they are proteolytically degraded to constituent amino acids (Ambroso *et al.* 1997; Brent and Fawcett 1998). The reported significant decreases in the clearance of FITC from media supplied FITC-albumin, as a result of EtOH exposure, corroborate previous studies that show similar EtOH effects on the VYS (Steventon and Williams 1987; Xu 2005). Based on the lack of a proportional increase of the acid-insoluble fraction in the VYS, we conclude that the effect of EtOH on HNP function is due to a direct effect on RME activity and not on the subsequent proteolysis step. The RME process is initiated by the binding of an exogenous bulk or carrier protein to the multiligand receptor complex that includes the principle proteins megalin and cubilin (Christensen and Birn 2002). Megalin and cubilin have been shown to coimmunolocalize in the human yolk sac in a similar manner, suggesting an analogous functional role of the VYS in the rodent model, despite obvious differences between human and rodent VYS structure and orientation (Burke *et al.* 2013).

Protein binding initiates a series of events that integrates activities of essential membrane proteins and the rearrangement of the actin cytoskeleton to initiate endocytosis and formation of the primary vesicle. The actin cytoskeleton and its dynamic regulation is a known target of EtOH toxicity (Loureiro *et al.* 2011; Oyedele and Kramer 2013; Romero *et al.* 2010). It is unlikely that EtOH acts directly to affect disruption of actin dynamics but the increased generation of ROS is believed to play an important role (Sakai *et al.* 2012). The observed oxidation of GSH in the VYS coupled with the significantly more positive E_h values (Fig. 7) are consistent with a role for increased ROS and altered redox regulation. These correlations are also supported by findings from the analysis of ICAT thiol proteomic data (Fig. 8) where a decreased abundance of several actin-related proteins (Arp2, profilin, and α-actinin) was identified. These proteins are known to play important roles in actin nucleation, branching, and depolymerization. All of these proteins must be regulated to facilitate endocytosis and cell migration, as well as other necessary structural functions that are important during the preimplantation stage and early embryonic development (Lassing *et al.* 2007; Sun *et al.* 2013). Because most of these dynamic changes have been associated with increased ROS or oxidative stresses, it is reasonable to suggest that redox-related posttranslational alterations to these proteins may contribute significantly to the observed reduction in RME activity. The relative abundance of β-actin is only decreased by 8% (Supplemental Fig. 1) following short-term EtOH exposure, which is consistent with changes to signaling machinery and not just actin availability. Furthermore, thioredoxin-1 (Trx-1), which has been shown to maintain the redox state of actin via reduction of oxidized thiols in cells under conditions of oxidative stress (Wang *et al.* 2010) was also shown to be significantly depleted in the VYS as a result of EtOH exposure (Fig. 8). Sensitivity to cellular redox disruption via posttranslational modification is additionally evidenced by S-glutathionylation of β-actin (cytosolic isoform) and profilin, which is a key protein in G-actin sequestration and microfilament dynamics (Fratelli *et al.* 2003).

Redox profile data from this study show the effects of increasing EtOH concentrations on GSH and Cys content and redox state in the major tissues (VYS, EMB) and major fluid compartments (YSF, AF) of the rat conceptus (Figs. 3–6). No attempts were made to directly quantify ROS, relying on sustained changes to the soluble thiol steady states to assess redox status. EtOH, at the concentrations used, did not cause significant reductions in total GSH (GSH + 2GSSG) in the VYS and AF, but did produce small decreases in the EMB and YSF. Traditional evidence for "oxidative stress" would interpret these results as EtOH having little or no effect on redox status. Further examination shows that significant decreases in GSH occur at 1.5 mg/ml EtOH and that corresponding values of GSSG significantly increase over the entire EtOH concentration range in VYS, EMB, and YSF. There did not appear to be as consistent or extensive pattern of GSH and Cys movement between tissue and fluid compartments as we have reported with other chemical modulators (Harris *et al.* 2013). In VYS and EMB, GSSG concentrations increased approximately 2-fold at all dose groups when compared with control levels (Fig. 5). This is likely attributable to oxidation of GSH to the disulfide form, as well as consistent shuttling of GSSG into the extracellular compartments (YSF and AF) (Ballatori *et al.* 2009). These results show evidence for the net oxidation of GSH to GSSG, which is confirmed by E_h values increasing by 18–41 mV (Fig. 7). The observed magnitude of redox change in these tissues and fluid compartment is consistent with studies reporting significant oxidative posttranslational modification of cysteine thiols. Based on these results, it is difficult to draw conclusions regarding the potential deleterious consequences of ROS elevation following EtOH, although, changes in E_h do indicate a permissive environment for redox signaling changes. (Jones 2006; Paulsen and Carroll 2009; Schafer and Buettner 2001; Schieber and Chandel 2014).

The increased generation of ROS has been discussed previously in relation to the disruption of HNP functions and cytoskeletal dynamics. Because of the vast number of oxidizable protein thiols present in cells and tissues, the magnitude of ROS-induced changes is daunting. Disruption of the cellular cysteine redox circuitry has many important implications in biochemical and physiological signaling pathways that also require input from cellular metabolism as with the supply of reducing equivalents. Functional Trx-1 was previously identified as a critical redox-regulating enzyme that is reduced in abundance following EtOH treatment (Karshikoff *et al.* 2013). Maintenance of Trx-1 in its reduced and active state is dependent on thioredoxin reductase, which receives electrons from NADPH, its obligate electron donor. Transcriptomic studies in embryonic mouse models have shown that the pentose phosphate pathway is upregulated in response to EtOH exposure in resistant strains (B6N), indicating a possible adaptive response in supplying additional NADPH as reducing equivalents (Green *et al.* 2007) Additionally, the glutaredoxin system, when balanced with physiologically relevant concentrations of GSH, NADPH, and GSH reductase, has been shown to protect against Trx-1 active site oxidation (Du *et al.* 2013). Although both systems are distinct redox circuits, the depletion of reduced GSH and reducing equivalents due to EtOH exposure may hinder the cells ability to maintain adequate levels of reduced Trx-1. Thus, this demonstrates that the ROS-generating capacity of EtOH may target specific cellular signaling pathways, outside of the scope of general oxidative damage to cells and tissues.

Although several correlations were found to exist between redox status, HNP activity and potential connections to redox signaling and circuitry in the context of EtOH embryotoxicity, it

is also clear that many other potential pathways may be affected. A number of studies have found that ROS produced by EtOH metabolism can be linked to cell death via apoptosis (Sulik *et al.* 1981, 1988; Dunty *et al.* 2001), which is believed to be initiated when E_h values increase above −170 mV. Although programmed cell death pathways may be initiated as a result of increased ROS production, other responses having the exact opposite outcome are also known to be regulated by ROS. Pathway analysis (KEGG) of EtOH-induced changes to the thiol proteome revealed significant numbers of altered pathway elements mapping to the ribosome, protein folding, sorting, and degradation pathways (Fig. 8). These pathways are of particular interest because they are developmentally relevant, they are easily initiated as a result of nutrient amino acid deficiency (such as through HNP activity inhibition), and they are extensively redox regulated processes (Aburto *et al.* 2012; Cecconi and Levine 2008; Cecconi *et al.* 2008; Dodson *et al.* 2013; Zhang 2015). Recent studies on mechanisms of EtOH embryotoxicity have understandably focused on the brain and various aspects of neurotoxicity. A key element in many of these studies is the direct association between EtOH and the initiation of autophagy in neural tissues which may be expressed very differently in different species and strains of animals (Alimov *et al.* 2013; Luo 2014). This differential sensitivity to EtOH has been shown in mouse models for FASD where B6J dams were dosed twice, 4 h apart, on GD 8 with 2.9 g/kg EtOH, resulting in a significantly higher incidence of FASD outcomes when compared with identical exposures in the related B6N strains (Green *et al.* 2007). Microarray transcript profiling of the embryonic headfold (3-h post-EtOH exposure) from the resistant B6N strain showed downregulation of KEGG pathways for ribosomal proteins and proteosome and upregulation of glycolysis and pentose phosphate pathways. Actin cytoskeleton, focal adhesion, adherens junction, and other HNP-related genes were expressed and upgregulated in both mouse strains. We have observed similar affected pathways in our analysis of the thiol proteome suggesting central roles for autophagy and its related nutritional and redox-related control mechanisms. A final example from the thiol proteome analysis that shows a high degree of correlation with the ribosome and more general autophagy pathways is manifest by the observed decreased abundance of Ran cycle-related nuclear transport proteins, both in the EMB and VYS (Fig. 8). Several proteins involved in the Ran cycle have been previously shown to be redox-sensitive. Specifically, ROS has been shown to alter the GDP dissociation rate from Ran, due to its unique structure (Heo 2008). Ran cycles operate in both EMB and VYS to transport ribonucleoproteins (including 40S and 60S subunits) from the site of synthesis in the nucleolus to the cytosol (Kodiha *et al.* 2004; Miyamoto *et al.* 2004); Failure of this system results in accumulation of ribosomal and preribosomal material in the nucleus (Lounsbury and Macara 1997). Thus, the abundance of several other downstream proteins may be affected as a result of an altered Ran-GTPase cycle or decreased recycling of Ran proteins; such proteins may lie outside of the thiol proteome or may exist in low abundance, effectively being missed by the ICAT procedure. Furthermore, the intracellular domains of EGFR-family proteins have been found to be proteolytically cleaved following ligand binding, then acting as transcription factors. Many of these, including EGFR and ErbB2, have been shown to be translocated into the nucleus by importin-β, which is dependent on the Ran cycle (Wang and Hung 2009). The resulting collapse of the Ran gradient also results in the accumulation of importin-α (Kodiha *et al.* 2004; Miyamoto *et al.* 2004). Additionally, Ran, nucleoporin Nup153, and importin-β are also proteolytically degraded under conditions of oxidative stress (Kodiha *et al.* 2004), consistent with our proteomic data in the VYS. Alternatively, although we did not observe direct alterations to Ran in the EMB, our proteomic data (Fig. 8) shows that Ran binding protein-1 (RanBP1) abundance is significantly reduced in the treatment group. This may, likewise, be indicative of a collapse of the Ran cycle, as RanBP1 has been found to reduce inhibition of Ran GTPase-activating protein (RanGAP) (Lounsbury and Macara 1997) and is required for hydrolysis of Ran-bound GTP (Petersen *et al.* 2000), completing the Ran cycle and maintaining the Ran concentration gradient necessary for nuclear transport. It is also important to note that the Ran nuclear translocation activities are integral to the ribosome biosynthesis pathways that make ribonucleotides in the nucleoli and transport them to the cytosol for ribosome assembly and function (Fromont-Racine *et al.* 2003; Johnson *et al.* 2002), which is suggested as a targeted pathway by our data (Fig. 8). Nuclear import/export pathways are important in development because of the significant roles they play in mediating the EtOH-induced disruption of cell transport, signaling, mitosis, and cell cycle progression (Dasso 2002).

In conjunction with existing evidence, our data suggest some novel insights into the mechanism of EtOH teratogenicity during early organogenesis. We have shown that EtOH alters the compartmentalized redox environments of the rodent conceptus, and have found this to be related to a significant, dose-dependent inhibition of HNP activity. These data demonstrate differential EtOH-induced effects in the EMB and VYS, and suggest that the VYS plays an important role during early organogenesis and is a distinct target for EtOH toxicity (Fig. 7). The resulting exacerbated conditions of intracellular oxidation may also contribute directly to significant changes in the functional thiol proteome as well as significant changes in the absolute amounts of critical proteins. Because our ICAT proteomic analysis only focused on the top 2.5% of most abundant proteins, we are certain there is much to yet be learned as we are able to mine deeper into changes involving less abundant proteins. Observed decreases for specific proteins involved in cytoskeletal dynamics and endocytosis (α-actinin, α-tubulin, cubilin, and actin-related protein 2), nuclear translocation (Ran and RanBP1), and maintenance of RME (cubilin) show direct correlation with functional changes in redox status and HNP activity. The combined alterations of HNP activity, ROS generation, and redox signaling and circuitry all impact the broader activation of autophagy pathways and may contribute significantly to the overall process of ribosome biogenesis, assembly and function that presents an interesting target for future studies in EtOH teratogenesis as have been shown in specific studies focused on mechanisms of EtOH neurogenesis (Luo 2014).

SUPPLEMENTARY DATA

Supplementary data are available online at http://toxsci.oxfordjournals.org/.

FUNDING

This work was supported by the Bill and Melinda Gates Foundation, Grand Challenges Explorations, Round 7; the University of Michigan National Institute of Environmental Health Sciences (NIEHS) Core Center, "Lifestage Exposures and Adult Disease" (P30 ES017885); and from an

Institutional Training Grant from the NIEHS to K.E.S. (T32 ES007062).

ACKNOWLEDGMENTS

The authors thank Ofra Duchen, Thomas J. Wolfe, and Anthony Su for contributing to the production and analysis of data supporting this work. The findings and conclusions in this manuscript are those of the authors and do not necessarily represent the official views or policies of the Centers for Disease Control and Prevention.

References

Aburto, M. R., Hurlé, J. M., Varela-Nieto, I., and Magariños, M. (2012). Autophagy during vertebrate development. *Cells* **1**, 428–448.

Alimov, A., Wang, H., Liu, M., Frank, J., Xu, M., Ou, X., and Luo, J. (2013). Expression of autophagy and UPR genes in the developing brain during ethanol-sensitive and resistant periods. *Metab. Brain Dis.* **28**, 667–676.

Ambroso, J., and Harris, C. (2012). Assessment of histiotrophic nutrition using fluorescent probes. *Methods Mol. Biol.* **889**, 407–423.

Ambroso, J. L., and Harris, C. (1993). Chloroquine embryotoxicity in the postimplantation rat conceptus in vitro. *Teratology* **48**, 213–226.

Ambroso, J. L., Larsen, S. V., Brabec, R. K., and Harris, C. (1997). Fluorometric analysis of endocytosis and lysosomal proteolysis in the rat visceral yolk sac during whole embryo culture. *Teratology* **56**, 201–209.

Arriazu, E., Pérez de Obanos, M. P., López-Zabalza, M. J., Herraiz, M. T., and Iraburu, M. J. (2010). Amino acid deprivation decreases intracellular levels of reactive oxygen species in hepatic stellate cells. *Cell. Physiol. Biochem.* **26**, 281–290.

Balaraman, S., Tingling, J. D., Tsai, P. C., and Miranda, R. C. (2013). Dysregulation of microRNA expression and function contributes to the etiology of fetal alcohol spectrum disorders. *Alcohol Res.* **35**, 18–24.

Ballatori, N., Krance, S. M., Marchan, R., and Hammond, C. L. (2009). Plasma membrane glutathione transporters and their roles in cell physiology and pathophysiology. *Mol. Aspects Med.* **30**, 13–28.

Beckman, D. A., Lloyd, J. B., and Brent, R. L. (1998). Quantitative studies on the mechanisms of amino acid supply to rat embryos during organogenesis. *Reprod. Toxicol.* **12**, 197–200.

Brent, R. L., Beckman, D. A., Jensen, M., and Koszalka, T. R. (1990). Experimental yolk sac dysfunction as a model for studying nutritional disturbances in the embryo during early organogenesis. *Teratology* **41**, 405–413.

Brent, R. L., and Fawcett, L. B. (1998). Nutritional studies of the embryo during early organogenesis with normal embryos and embryos exhibiting yolk sac dysfunction. *J. Pediatr.* **132**, S6–S16.

Burke, K. A., Jauniaux, E., Burton, G. J., and Cindrova-Davies, T. (2013). Expression and immunolocalisation of the endocytic receptors megalin and cubilin in the human yolk sac and placenta across gestation. *Placenta* **34**, 1105–1109.

Burton, G. J., Hempstock, J., and Jauniaux, E. (2001). Nutrition of the human fetus during the first trimester–a review. *Placenta* **22**(Suppl. A), S70–S77.

Cecconi, F., and Levine, B. (2008). The role of autophagy in mammalian development: Cell makeover rather than cell death. *Dev. Cell* **15**, 344–357.

Cecconi, F., Piacentini, M., and Fimia, G. M. (2008). The involvement of cell death and survival in neural tube defects: A distinct role for apoptosis and autophagy? *Cell Death Differ.* **15**, 1170–1177.

Chen, X., Liu, J., and Chen, S. Y. (2013). Sulforaphane protects against ethanol-induced oxidative stress and apoptosis in neural crest cells by the induction of Nrf2-mediated antioxidant response. *Br. J. Pharmacol.* **169**, 437–448.

Christensen, E. I., and Birn, H. (2002). Megalin and cubilin: Multifunctional endocytic receptors. *Nat. Rev. Mol. Cell Biol.* **3**, 256–266.

Chung, H. S., Wang, S.-B., Venkatraman, V., Murray, C. I., and Van Eyk, J. E. (2013). Cysteine oxidative posttranslational modifications: Emerging regulation in the cardiovascular system. *Circ. Res.* **112**, 382–392.

Coriale, G., Fiorentino, D., Di Lauro, F., Marchitelli, R., Scalese, B., Fiore, M., Maviglia, M., and Ceccanti, M. (2013). Fetal alcohol spectrumdisorder (FASD): Neurobehavioral profile, indications for diagnosis and treatment. *Riv. Psichiatr.* **48**, 359–369.

Dasso, M. (2002). The Ran GTPase: Theme and variations. *Curr. Biol.* **12**, R502–R508.

Davis, W. L. (1990). Ethanol induces the generation of reactive free radicals by neural crest cells in vitro. *J. Craniofac. Genet. Dev. Biol.* **10**, 277–293.

Dodson, M., Darley-Usmar, V., and Zhang, J. (2013). Cellular metabolic and autophagic pathways: Traffic control by redox signaling. *Free Radic. Biol. Med.* **63**, 207–221.

Dong, J., Sulik, K. K., and Chen, S. Y. (2008). Nrf2-mediated transcriptional induction of antioxidant response in mouse embryos exposed to ethanol in vivo: Implications for the prevention of fetal alcohol spectrum disorders. *Antioxid. Redox Signal.* **10**, 2023–2033.

Dong, J., Sulik, K. K., and Chen, S. Y. (2010). The role of NOX enzymes in ethanol-induced oxidative stress and apoptosis in mouse embryos. *Toxicol. Lett.* **193**, 94–100.

Dreosti, I. E. (1993). Nutritional factors underlying the expression of the fetal alcohol syndrome. *Ann. N. Y. Acad. Sci.* **678**, 193–204.

Du, Y., Zhang, H., Zhang, X., Lu, J., and Holmgren, A. (2013). Thioredoxin 1 is inactivated due to oxidation induced by peroxiredoxin under oxidative stress and reactivated by the glutaredoxin system. *J. Biol. Chem.* **288**, 32241–32247.

Dunty, W. C., Jr, Chen, S. Y., Zucker, R. M., Dehart, D. B., and Sulik, K. K. (2001). Selective vulnerability of embryonic cell populations to ethanol-induced apoptosis: Implications for alcohol-related birth defects and neurodevelopmental disorder. *Alcohol. Clin. Exp. Res.* **25**, 1523–1535.

Finkel, T. (2011). Signal transduction by reactive oxygen species. *J. Cell Biol.* **194**, 7–15.

Fratelli, M., Demol, H., Puype, M., Casagrande, S., Villa, P., Eberini, I., Vandekerckhove, J., Gianazza, E., and Ghezzi, P. (2003). Identification of proteins undergoing glutathionylation in oxidatively stressed hepatocytes and hepatoma cells. *Proteomics* **3**, 1154–1161.

Fromont-Racine, M., Senger, B., Saveanu, C., and Fasiolo, F. (2003). Ribosome assembly in eukaryotes. *Gene* **313**, 17–42.

Fu, C., Hu, J., Liu, T., Ago, T., Sadoshima, J., and Li, H. (2008). Quantitative analysis of redox-sensitive proteome with DIGE and ICAT. *J. Proteome Res.* **7**, 3789–3802.

Go, Y.-M., Roede, J. R., Orr, M., Liang, Y., and Jones, D. P. (2014). Integrated redox proteomics and metabolomics of mitochondria to identify mechanisms of Cd toxicity. *Toxicol. Sci.* **139**, 59–73.

Green, M. L., Singh, A. V., Zhang, Y., Nemeth, K. A., Sulik, K. K., and Knudsen, T. B. (2007). Reprogramming of genetic networks during initiation of the fetal alcohol syndrome. *Dev. Dyn.* **236**, 613–631.

Guttmann, R. P. (2010). Redox regulation of cysteine-dependent enzymes. *J. Anim. Sci.* **88**, 1297–1306.

Hansen, J. M., and Harris, C. (2013). Redox control of teratogenesis. *Reprod. Toxicol.* **35**, 165–179.

Harris, C. (2012). Rodent whole embryo culture. *Methods Mol. Biol.* **889**, 215–237.

Harris, C., and Hansen, J. (2012). Oxidative stress, thiols, and redox profiles. In: *Developmental Toxicology* (C. Harris and J. M. Hansen, Eds.), pp. 325–346. Humana Press, NY, New York.

Harris, C., Shuster, D. Z., Roman Gomez, R., Sant, K. E., Reed, M. S., Pohl, J., and Hansen, J. M. (2013) Inhibition of glutathione biosynthesis alters compartmental redox status and the thiol proteome in organogenesis-stage rat conceptuses. *Free Radic. Biol. Med.* **63**, 325–337.

Heo, J. (2008). Redox regulation of Ran GTPase. *Biochem. Biophys. Res. Commun.* **376**, 568–572.

Hill, A. J., Drever, N., Yin, H., Tamayo, E., Saade, G., and Bytautiene, E. (2014). The role of NADPH oxidase in a mouse model of fetal alcohol syndrome. Am. J. Obstet. Gynecol. **210**, 466.e1–466.e5.

Johnson, A. W., Lund, E., and Dahlberg, J. (2002). Nuclear export of ribosomal subunits. *Trends Biochem. Sci.* **27**, 580–585.

Jones, D. P. (2002). [11] Redox potential of GSH/GSSG couple: Assay and biological significance. In: *Methods in Enzymology* (S. Helmut and P. Lester, Eds.), pp. 93–112. Academic Press, San Diego, CA.

Jones, D. P. (2006). Redefining oxidative stress. *Antioxid. Redox Signal.* **8**, 1865–1879.

Kaminen-Ahola, N., Ahola, A., Maga, M., Mallitt, K. A., Fahey, P., Cox, T. C., Whitelaw, E., and Chong, S. (2010). Maternal ethanol consumption alters the epigenotype and the phenotype of offspring in a mouse model. *PLoS Genet.* **6**, e1000811.

Karshikoff, A., Nilsson, L., and Foloppe, N. (2013). Understanding the -C-X1-X2-C- motif in the active site of the thioredoxin superfamily: *E. coli* DsbA and its mutants as a model system. *Biochemistry* **52**, 5730–5745.

Kirlin, W. G., Cai, J., Thompson, S. A., Diaz, D., Kavanagh, T. J., and Jones, D. P. (1999). Glutathione redox potential in response to differentiation and enzyme inducers. *Free Radic. Biol. Med.* **27**, 1208–1218.

Kodiha, M., Chu, A., Matusiewicz, N., and Stochaj, U. (2004). Multiple mechanisms promote the inhibition of classical nuclear import upon exposure to severe oxidative stress. *Cell Death Differ.* **11**, 862–874.

Lassing, I., Schmitzberger, F., Bjornstedt, M., Holmgren, A., Nordlund, P., Schutt, C. E., and Lindberg, U. (2007). Molecular and structural basis for redox regulation of beta-actin. *J. Mol. Biol.* **370**, 331–348.

Lounsbury, K. M., and Macara, I. G. (1997). Ran-binding protein 1 (RanBP1) forms a ternary complex with Ran and karyopherin beta and reduces Ran GTPase-activating protein (RanGAP) inhibition by karyopherin beta. *J. Biol. Chem.* **272**, 551–555.

Loureiro, S. O., Heimfarth, L., Reis, K., Wild, L., Andrade, C., Guma, F. T. C. R., Gonçalves, C. A., and Pessoa-Pureur, R. (2011). Acute ethanol exposure disrupts actin cytoskeleton and generates reactive oxygen species in c6 cells. *Toxicol.in vitro* **25**, 28–36.

Luo, J. (2014). Autophagy and ethanol neurotoxicity. *Autophagy* **10**, 2099–2108.

Miller, L., Shapiro, A. M., Cheng, J., and Wells, P. G. (2013). The free radical spin trapping agent phenylbutylnitrone reduces fetal brain DNA oxidation and postnatal cognitive deficits caused by in utero exposure to a non-structurally teratogenic dose of ethanol: A role for oxidative stress. *Free Radic. Biol. Med.* **60**, 223–232.

Miller-Pinsler, L., Pinto, D. J., and Wells, P. G. (2015). Oxidative DNA damage in the in utero initiation of postnatal neurodevelopmental deficits by normal fetal and ethanol-enhanced oxidative stress in oxoguanine glycosylase 1 knockout mice. *Free Radic. Biol. Med.* **78**, 23–29.

Miyamoto, Y., Saiwaki, T., Yamashita, J., Yasuda, Y., Kotera, I., Shibata, S., Shigeta, M., Hiraoka, Y., Haraguchi, T., and Yoneda, Y. (2004). Cellular stresses induce the nuclear accumulation of importin α and cause a conventional nuclear import block. *J. Cell Biol.* **165**, 617–623.

Mukherjee, R. A. S., Hollins, S., and Turk, J. (2006). Fetal alcohol spectrum disorder: An overview. *J. R. Soc. Med.* **99**, 298–302.

Oyedele, O. O., and Kramer, B. (2013). Nuanced but significant: How ethanol perturbs avian cranial neural crest cell actin cytoskeleton, migration and proliferation. Alcohol. **47**, 417–426.

Park, P. H., Miller, R., and Shukla, S. D. (2003). Acetylation of histone H3 at lysine 9 by ethanol in rat hepatocytes. *Biochem. Biophys. Res. Commun.* **306**, 501–504.

Paulsen, C. E., and Carroll, K. S. (2009). Orchestrating redox signaling networks through regulatory cysteine switches. *ACS Chem. Biol.* **5**, 47–62.

Petersen, C., Orem, N., Trueheart, J., Thorner, J. W., and Macara, I. G. (2000). Random mutagenesis and functional analysis of the Ran-binding protein, RanBP1. *J. Biol. Chem.* **275**, 4081–4091.

Romero, A. M., Esteban-Pretel, G., Marín, M. P., Ponsoda, X., Ballestín, R., Canales, J. J., and Renau-Piqueras, J. (2010). Chronic ethanol exposure alters the levels, assembly, and cellular organization of the actin cytoskeleton and microtubules in hippocampal neurons in primary culture. *Toxicol. Sci.* **118**, 602–612.

Sakai, J., Li, J., Subramanian Kulandayan, K., Mondal, S., Bajrami, B., Hattori, H., Jia, Y., Dickinson Bryan, C., Zhong, J., Ye, K., *et al.* (2012). Reactive oxygen species-induced actin glutathionylation controls actin dynamics in neutrophils. *Immunity* **37**, 1037–1049.

Schafer, F. Q., and Buettner, G. R. (2001). Redox environment of the cell as viewed through the redox state of the glutathione disulfide/glutathione couple. *Free Radic. Biol. Med.* **30**, 1191–1212.

Schieber, M., and Chandel Navdeep, S. (2014). ROS function in redox signaling and oxidative stress. *Curr. Biol.* **24**, R453–R462.

Smith, S. M. (1997). Alcohol-induced cell death in the embryo. *Alcohol Health Res. World* **21**, 287–297.

Steventon, G. B., and Williams, K. E. (1987). Ethanol-induced inhibition of pinocytosis and proteolysis in rat yolk sac in vitro. *Development* **99**, 247–253.

Sulik, K. K., Cook, C. S., and Webster, W. S. (1988). Teratogens and craniofacial malformations: Relationships to cell death. *Development* **103**(Suppl.), 213–231.

Sulik, K. K., Johnston, M. C., and Webb, M. A. (1981). Fetal alcohol syndrome: Embryogenesis in a mouse model. *Science* **214**, 936–938.

Sun, S. C., Wang, Q. L., Gao, W. W., Xu, Y. N., Liu, H. L., Cui, X. S., and Kim, N. H. (2013). Actin nucleator Arp2/3 complex is essential for mouse preimplantation embryo development. *Reprod. Fertil. Dev.* **25**, 617–623.

Ungerer, M., Knezovich, J., and Ramsay, M. (2013). In utero alcohol exposure, epigenetic changes, and their consequences. *Alcohol Res*. **35**, 37–46.

Wang, L. L., Zhang, Z., Li, Q., Yang, R., Pei, X., Xu, Y., Wang, J., Zhou, S. F., and Li, Y. (2009). Ethanol exposure induces differential microRNA and target gene expression and teratogenic effects which can be suppressed by folic acid supplementation. *Hum. Reprod*. **24**, 562–579.

Wang, S. C., and Hung, M. C. (2009). Nuclear translocation of the epidermal growth factor receptor family membrane tyrosine kinase receptors. *Clin. Cancer Res*. **15**, 6484–6489.

Wang, X., Ling, S., Zhao, D., Sun, Q., Li, Q., Wu, F., Nie, J., Qu, L., Wang, B., Shen, X., *et al*. (2010). Redox regulation of actin by thioredoxin-1 is mediated by the interaction of the proteins via cysteine 62. *Antioxid. Redox Signal*. **13**, 565–573.

Xu, Y. (2005). Effect of ethanol on the development of visceral yolk sac. *Hum. Reprod*. **20**, 2509–2516.

Zhang, J. (2015). Teaching the basics of autophagy and mitophagy to redox biologists—Mechanisms and experimental approaches. *Redox Biol*. **4**, 242–259.